ACS APPLIED MATERIALS & INTERFACES

Research Article

www.acsami.org

# Dynamic Characteristics of Aggregation Effects of Organic Dyes in Dye-Sensitized Solar Cells

Shuai Feng,[†,‡] Quan-Song Li,[*,†] Ping-Ping Sun,[†] Thomas A. Niehaus,[§] and Ze-Sheng Li[†]

[†]Beijing Key Laboratory of Photoelectronic/Electrophotonic Conversion Materials, Key Laboratory of Cluster Science of Ministry of Education, School of Chemistry, Beijing Institute of Technology, Beijing 100081, China

[‡]College of Chemistry and Chemical Engineering, Taishan University, Taian 271021, China

[§]Department of Theoretical Physics, University of Regensburg, 93040 Regensburg, Germany

Supporting Information

**ABSTRACT:** Two organic dyes (LS-1 and $IQ_4$) containing identical electron donor and acceptor units but distinct $\pi$ units result in significantly different power conversion efficiency of the corresponding dye-sensitized solar cells (DSSCs): LS-1, 4.4%, and $IQ_4$, 9.2%. Herein, we combine first-principle calculations and molecular dynamics to explore the aggregation effects of LS-1 and $IQ_4$ by comparing their optical properties and intermolecular electronic couplings. The calculated absorption spectra are in good agreement with the experimental observations and reveal them to be evidently affected by the dimerization. Furthermore, molecular dynamics simulations show that steric hindrance induced by the diphenylquinoxaline unit in $IQ_4$ can elongate the distances between intermolecular $\pi$ units or electron donors, which are responsible for the fact that the intermolecular electronic coupling of LS-1 is about 10 times larger than that of $IQ_4$. More importantly, the aggregated $IQ_4$ remains almost perpendicular to the $TiO_2$ surface, whereas LS-1 gradually tilts during the dynamic simulation, impacting electron injection and recombination in several ways, which clarifies why $IQ_4$ leads to larger photocurrent and higher conversion efficiency. The deep understanding of the dye aggregation effects sheds new light on the complex factors determining DSSC function and paves the way for rational design of high-efficiency self-anti-aggregation sensitizers.

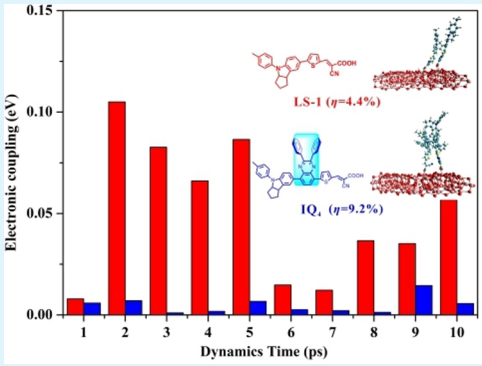


**KEYWORDS:** *dye-sensitized solar cell, aggregation effects, optical property, molecular dynamics, electronic coupling*

## 1. INTRODUCTION

Dye-sensitized solar cells (DSSCs) have been considered as potential low-cost high-efficiency alternatives to replace the traditional silicon-based photovoltaics for a few decades.[1−4] As the most critical component in DSSCs, dye-sensitizers take part in light absorption, charge injection, dye regeneration, and charge recombination, which are key processes regulating the power conversion efficiency (PCE, $\eta$).[3,5] Compared with organometallic dyes containing zinc (Zn) and ruthenium (Ru), organic dyes with the common donor−$\pi$ linker−acceptor (D−$\pi$−A) configuration possess various merits such as easy synthesis, facile structure modification, and abundance.[5−8] Recently, the photovoltaic performance of DSSCs employing pure metal-free organic dyes has achieved 12.5%,[9] close to the DSSCs record of 13% based on Zn(II) porphyrins.[4] Nevertheless, the PCE of metal-free DSSC is generally under 9% and lower than those based on Ru complexes[10,11] and Zn(II) porphyrins.[4]

Most organic dyes are prone to form aggregates on the photoanode (typically nanocrystalline $TiO_2$) because of electrostatic and noncovalent interactions of adjacent dye molecules. Although some aggregates are reported to be benign because the formed compact dye layer on the $TiO_2$ surface can extend the light absorption window and suppress electron recombination between the injected electron and the electrolyte,[12,13] the strong intermolecular interaction within the compact dye layer leads to lateral charge transfer between the dye layers as well as excited-state quenching, which is adverse to the process of electron injection into the $TiO_2$ conduction band and thus reduces the photocurrent and the overall photovoltaic performance.[14,15]

To mitigate undesired dye aggregation in DSSCs, various approaches have been developed. One common method is the use of coadsorbents, typically deoxycholic acid (DCA) and chenodeoxycholic acid (CDCA), that compete with the dyes in the immersion process on $TiO_2$ and to some extent block the dye−dye interaction.[14,16,17] Meanwhile, the coadsorbents occupy some adsorption sites of the dye on the photoanode and lead to a consequent decrease in light-harvesting efficiency. Another effective way is the introduction of sterically hindered

**Received:** July 24, 2015
**Accepted:** September 22, 2015
**Published:** September 22, 2015





DOI: 10.1021/acsami.5b06743
ACS Appl. Mater. Interfaces 2015, 7, 22504−22514

groups on the molecular skeleton of the organic dyes, including the donor part,[18,19] the $\pi$ linker,[20,21] and the acceptor moiety.[22] However, incorporation of a long alkyl chain on the donor part has little antiaggregation effect,[19] and introduction of an alkyl chain on a thiophene linker may decrease the photostability of the device.[23] Additionally, a novel strategy to solve the aggregation problem has been put forward by inserting an additional electron-withdrawing unit between the electron-donor part and the $\pi$ framework, thus constructing D−A−$\pi$−A featured sensitizers.[24−33] The incorporated acceptors, such as diketopyrrolopyrrole,[24] benzothiadiazole,[25,26] benzotriazole,[27,28] and quinoxaline,[29−32] not only restrain the intermolecular aggregations via steric hindrance but also help to keep a balance between the open-circuit voltage ($V_{OC}$) and the short-circuit current density ($J_{SC}$) by modulating the energy levels of the frontier orbitals.

On the theoretical side, great efforts have been made with regard to the investigation of dye aggregation in DSSCs in terms of adsorption patterns, optical properties, and electronic structure. De Angelis and co-workers have systematically modeled a series of dye−dye intermolecular interactions taking place in DSSCs by modern first-principles computational methodologies.[34−41] They found that the dye−dye aggregation is of paramount importance in determining the overall DSSC conversion efficiency because the optical and electronic properties strongly depend on the aggregation patterns.[34−41] Zhang and Cole have studied the adsorption properties of *p*-methyl red monomeric-to-pentameric dye aggregates on anatase (101) $TiO_2$ surface via density functional theory (DFT) calculations.[42] Their results showed that monomer-to-tetrameric dye aggregates exhibit progressive red-shifting in the absorption spectra, whereas the pentameric form has a blue-shifted peak, suggesting that high-order aggregates beyond the dimer should be considered to fully understand the dye aggregation effects in DSSC.[42] Kusama and Sayama have carried out ab initio calculations on the intermolecular interactions in black dye dimers and black dye−DCA complexes.[43] The obtained results demonstrate that intermolecular hydrogen bonds were the main inducement for aggregation.[43] For our own part, we have carried out computational investigations on the aggregation effects of two indoline sensitizers, WS-2 and WS-6, which have identical molecular skeletons except that WS-6 bears an additional hexyl substitute resulting in 45% higher PCE.[44] We discovered that WS-2 is more prone to forming compact aggregates in solution and on $TiO_2$ surfaces and that the resulting strong aggregation interactions can induce larger electronic coupling between the stacked dimers, which may be detrimental for electronic injection from dye to $TiO_2$ and thus partly responsible for the loss of photovoltaic efficiency.[44] Clearly, theoretical works have provided plentiful insights into the understanding of the aggregation effects and may assist the molecular engineering of novel efficient sensitizers. However, most of the optical and electronic properties were obtained on the basis of static models, and the dynamic effects that might be crucial in the charge transfer and energy transfer processes are lacking.

Herein, we report joint first-principles calculations and molecular dynamics (MD) simulations on the aggregation effects of two organic sensitizers, $IQ_4$ and LS-1. (See the chemical structures in Scheme 1.) As can be seen, $IQ_4$ has the same molecular framework as the typical D−$\pi$−A dye LS-1 but with an additional acceptor unit 2,3-diphenylquinoxaline interspersed, thus resulting in a D−A−$\pi$−A configuration.

**Scheme 1. Molecular Structures of LS-1 and $IQ_4$**

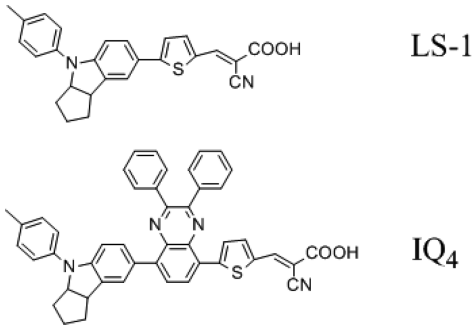


The $IQ_4$-based DSSCs display much better performance ($\eta$ = 9.24%, $V_{OC}$ = 0.74 V, $J_{SC}$ = 17.55 mA cm$^{-2}$, and *ff* = 0.71)[32] than that of the LS-1-based device ($\eta$ = 4.42%, $V_{OC}$ = 0.62 V, $J_{SC}$ = 11.25 mA cm$^{-2}$, and *ff* = 0.63).[27] Apart from some dissimilarities in solar cell structure and fabrication method, experimental observations suggest the main reasons for the different performance of the above-mentioned solar cells may come from distinct absorption coefficient (27 300 M$^{-1}$cm$^{-1}$ in $IQ_4$ and 20 100 M$^{-1}$cm$^{-1}$ in LS-1) and aggregation effect of the employed sensitizers. For coadsorption with 20 mM DCA, the conversion efficiency variations are different: $IQ_4$ reduces to $\eta$ = 8.18%, whereas LS-1 increases to $\eta$ = 4.72%, suggesting that $IQ_4$ possesses superior self-anti-aggregation character and that the aggregation effect in LS-1 is serious.[27,32]

Our results reveal that the two phenyl groups grafted onto the extra electron-withdrawing quinoxaline efficiently block the aggregations of adjacent dyes owing to steric restriction. MD simulations show that the dimeric configuration of $(IQ_4)_2$ remains almost perpendicular, whereas $(LS\text{-}1)_2$ dimers tend to tilt toward the $TiO_2$ surface, indicating different behavior for charge injection and recombination. Importantly, the intermolecular electronic coupling values of $(IQ_4)_2$ dimers within 10 ps of MD simulation are always smaller, and the average value is about 1/10 of that of $(LS\text{-}1)_2$ dimers, suggesting weaker intermolecular charge-transfer character and elucidating significant improvement in $J_{SC}$ of $IQ_4$-based DSSCs.

## 2. COMPUTATIONAL DETAILS

Density functional theory (DFT)[45,46] calculations have been carried out to optimize the ground-state geometries of isolated and dimeric dyes in solution using the B3LYP functional enhanced by dispersion corrections[47,48] with the 6-31G(d,p) basis set.[49] Dispersion corrections proposed by Grimme[48,50] can improve the accuracy of theoretical simulations for systems including noncovalent interactions, such as hydrogen bonding, $\pi$−$\pi$ stacking, and van der Waals interactions, which are ubiquitous and significant in dye aggregates in DSSCs. A normal-mode analysis is carried out at the same level of theory to confirm that the optimized geometries are minima on the potential energy surface. The $(TiO_2)_{124}$ cluster was constructed by clipping an anatase slab to show the (101) surface. The employed $(TiO_2)_{124}$ cluster, without unsaturated atoms or groups at the boundary, is an almost-square $TiO_2$ (101) two-layer anatase slab, with four rows of five- and six-coordinated surface Ti sites. To reduce computational cost, the geometries of dyes (monomers and dimers) adsorbed on the $TiO_2$ surface were optimized by the DFTB method.[51] The DFTB approach is an approximation of DFT based on a second-order expansion of the DFT total energy around a reference electron density. The SK-parameters of mio-1−1[46,52,53] for C, N, O, H, and S and tiorg-0−1[54] for Ti were employed. Molecular dynamics simulations of 10 ps duration have been carried out at $T$ = 298 K in the NVE ensemble with a time step of 1 fs with the DFTB+ 1.0.1 package.[51] For the


DOI: 10.1021/acsami.5b06743
ACS Appl. Mater. Interfaces 2015, 7, 22504−22514

absorption spectra, we carried out time-dependent DFT (TDDFT) calculations using the MPW1K hybrid density functional with 6-31G (d,p) basis set in $CH_2Cl_2$ solution. To reduce the computational efforts, the $(TiO_2)_{124}$ cluster was removed when simulating the absorption spectra on $TiO_2$. In the simplified model, the excitations between the dyes and $TiO_2$ will not be involved, thus probably leading to the absence of normally observed bathochromic shift in the absorption spectra of dyes adsorbed on $TiO_2$.[55] However, the compromising effects should be similar in cases of LS-1 and $IQ_4$, and our focus is on the relative band shifts upon aggregation. In DFT and TDDFT calculations, solvent effects were considered using the polarizable continuum model of solvation (C-PCM)[56] implemented in the Gaussian 09 code.[57]

The intermolecular electronic coupling ($V_{ij}$) is an important parameter for evaluating the coupling strength in aggregates. $V_{ij}$ can be estimated by the overlap of the frontier orbitals of the two adjacent molecules in a dimeric aggregate:[58]

$$V_{12} = \langle \varphi^1_{FMO} | H | \varphi^2_{FMO} \rangle$$

where $\varphi^1_{FMO}$ and $\varphi^2_{FMO}$ are the frontier molecular orbitals (FMO) of the two adjacent molecules 1 and 2. In this work, the FMO are approximated as the corresponding highest occupied molecular orbitals (HOMO). The $V_{ij}$ values were computed with two methods: the "energy splitting in dimer" (ESID) method and a direct approach.[59−62] Using the ESID method, on the basis of Koopmans' theorem,[63] the $V_{ij}$ were computed as one-half of the energy splitting of the two HOMO of the interacting monomers at the geometry that they have in the stable dimer. As for the direct method, the Fock operator (Kohn−Sham-Fock operator) in the dimer was used to evaluate the electronic coupling element, and its density matrix was constituted from noninteracting molecular orbitals.[62]

## 3. RESULTS AND DISCUSSION

**3.1. Structures and Optical and Electronic Properties in Solution.** The energy gap between the HOMO and the lowest unoccupied molecular orbital (LUMO) determines the optical absorption, polarizability, chemical reactivity, and kinetic stability of a molecule.[64] The energy levels and isosurfaces of HOMOs and LUMOs are depicted in Figure 1. It was reported that the HOMO−LUMO energy gap can be effectively decreased by incorporating an acceptor unit in the $\pi$ bridge, which results in a redshift of the electronic absorption spectra.[32] In Figure 1, the computed HOMO−LUMO energy gap of $IQ_4$ (2.09 eV) is smaller than that of LS-1 (2.44 eV), which is in line with the experimental observation.[32] Both HOMO and LUMO are of $\pi$ character and are delocalized over the molecular skeletons in LS-1 and $IQ_4$. However, the HOMO of $IQ_4$ is more localized on the donor part with respect to that of LS-1, where the HOMO partly spreads on the $\pi$ linker and the acceptor part, indicating a reduced overlap between HOMO and LUMO effected by incorporating the diphenylquinoxaline unit in $IQ_4$. In addition, the HOMO and LUMO extension on the two phenyl rings of the 2,3-diphenylquinoxaline moiety is negligible, suggesting the absorption spectra are not much influenced by the presence of the two phenyl rings. Note that the HOMOs are below the redox potential of the common redox couple $I^-/I_3^-$ and that the LUMOs are energetically higher than the conduction band edge of the frequently used semiconductor $TiO_2$ (Figure 1) which confirms that both LS-1 and $IQ_4$ are suitable to ensure the electron injection from the excited dye to $TiO_2$ and the dye regeneration by the redox couple in DSSCs. Furthermore, the contribution of the anchoring group (COOH) to HOMO and LUMO of LS-1 is 1.57 and 8.81%, respectively, whereas it is 0.2% to HOMO and 7.35% to LUMO in $IQ_4$. It is known that the contribution of anchoring group to LUMO strongly impacts the electron injection.[8] Thus, our results indicate comparable electron injection performances in LS-1 and $IQ_4$.

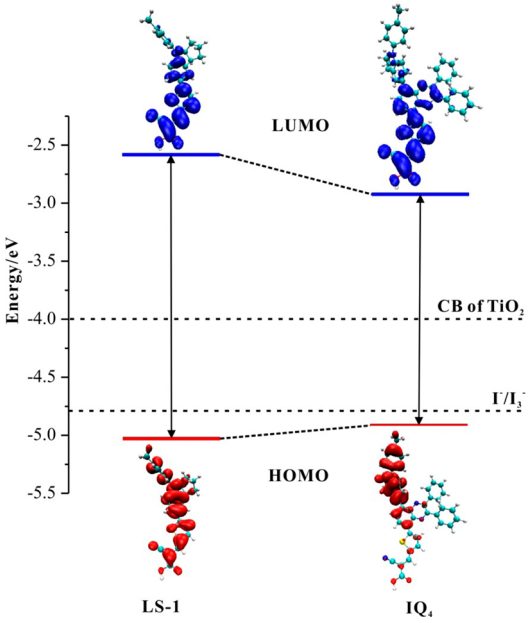


**Figure 1.** Calculated energy levels and isosurfaces of HOMOs (in red) and LUMOs (in blue) of LS-1 and $IQ_4$ in $CH_2Cl_2$ solution together with the experimental conduction band (CB) edge of $TiO_2$ and the redox potential of $I^-/I_3^-$.

The calculated absorption spectra of LS-1 and $IQ_4$ in $CH_2Cl_2$ are shown in Figure 2a,b. The calculated lowest excitation energy of $IQ_4$ (2.50 eV) is obviously red-shifted compared to that of LS-1 (2.59 eV), which agrees well with the experimental trend ($IQ_4$, 2.34 eV; LS-1, 2.57 eV).[27,32] The computed key parameters related to the optical properties of the two isolated dyes (LS-1 and $IQ_4$) in $CH_2Cl_2$ solution are summarized in Table 1. It is noticed that the lowest excitation energies of LS-1 and $IQ_4$ exhibit large oscillator strengths and correspond essentially to HOMO−LUMO excitations. Moreover, $IQ_4$ shows an additional absorption band around 3.22 eV (~385 nm) (Figure 2b), which ensures effective light harvesting in this region. However, the calculated lowest excitation energy of isolated $IQ_4$ (2.50 eV) is overestimated compared to the experimental result (2.34 eV), implying that aggregates more than the monomers should be taken into account for better assignment of the absorption spectra. Next, we will further study the optical properties of the dimers to get more insights into the absorption spectra.

For the dimers of LS-1 and $IQ_4$ in solution, we have considered the two most possible configurations as shown in Figure S1: one is the face-to-face stacking pattern (pattern A), and the other one is the face-to-back stacking pattern (pattern B), where one dye is rotated by 180° around the long axis with respect to dimer A. The dye aggregates in $CH_2Cl_2$ solution are labeled as $(LS\text{-}1)_2$-A, $(LS\text{-}1)_2$-B, $(IQ_4)_2$-A, and $(IQ_4)_2$-B, respectively. The interaction energies ($\Delta E$) of dye dimers in $CH_2Cl_2$ solution are listed in Table S1, which are computed as the difference between the total energy of the dimer and twice the energy of the isolated molecules. It is apparent that the $\Delta E$ of $(LS\text{-}1)_2$ dimers (−1.21 and −1.19 eV) are much smaller than those of $(IQ_4)_2$ dimers (−2.28 and −2.23 eV), indicating that


DOI: 10.1021/acsami.5b06743
ACS Appl. Mater. Interfaces 2015, 7, 22504−22514

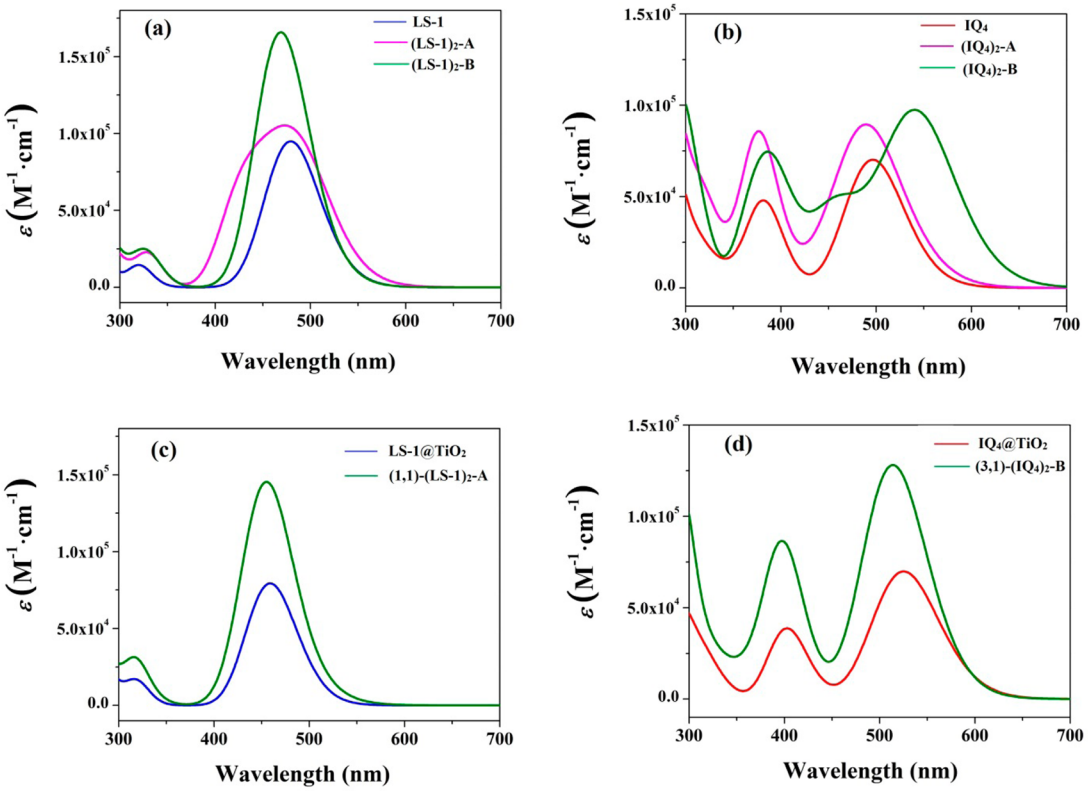


**Figure 2.** Calculated absorption spectra of monomers and dimers: (a) LS-1 in $CH_2Cl_2$ solution, (b) $IQ_4$ in $CH_2Cl_2$ solution, (c) LS-1 adsorbed on $TiO_2$ surface, and (d) $IQ_4$ adsorbed on $TiO_2$ surface.

**Table 1. Computed TDDFT(MPW1K)/6-31G(d,p) Excitation Energies ($E$), Oscillator Strengths ($f$), and Dominant Excitation Configurations for the Lowest Excited State ($S_1$) in $CH_2Cl_2$ Solution at the Geometry Optimized by B3LYP/6-31G(d,p)**

| monomer | | $E$ (eV) | $f$ | $\lambda_{max}$ (nm) | MO character |
|---|---|---|---|---|---|
| LS-1 | $S_1$ | 2.59 | 1.309 | 478.9 | HOMO→LUMO (68.8%) |
| $IQ_4$ | $S_1$ | 2.50 | 0.968 | 496.1 | HOMO→LUMO (65.3%) |
| LS-1[a] | $S_1$ | 2.57 | | 483 | |
| $IQ_4$[b] | $S_1$ | 2.34 | | 529 | |

[a]Experimental data in $CH_2Cl_2$ solution from reference 27. [b]Experimental data in $CH_2Cl_2$ solution from reference 32.

the additional 2,3-diphenylquinoxaline group contributes a lot to the intermolecular interaction.

It is noticeable that in Figure 2b that the strongest absorption band moves to around 550 nm in $(IQ_4)_2$-B compared to that of the isolated $IQ_4$. As listed in Table 2, the $S_1$ state of dimers $(LS\text{-}1)_2$-A, $(LS\text{-}1)_2$-B, $(IQ_4)_2$-A, and $(IQ_4)_2$-B are located at 2.42, 2.48, 2.35, and 2.20 eV, respectively. Note that the lowest excitation energies of $(LS\text{-}1)_2$ dimers are slightly shifted (Figure 2a) and vary from 2.59 eV in isolated LS-1 to 2.55 eV for $(LS\text{-}1)_2$-A and to 2.65 eV for $(LS\text{-}1)_2$-B. Interestingly, a different optical response is observed for $(IQ_4)_2$ dimers: The band maximum moves from 2.50 eV in monomeric $IQ_4$ to 2.52 eV for $(IQ_4)_2$-A, exhibiting a slight blueshift, whereas for $(IQ_4)_2$-B, an obvious redshift of about −0.20 eV is found (Figure 2b). Furthermore, the $S_2$ state of $(IQ_4)_2$-B located at 2.30 eV is close to the experimental $\lambda_{max}$ (2.34 eV),[32] which implies that $(IQ_4)_2$-B may exist in solution and features a broadened light-absorption window that is a favorable effect with regard to the conversion efficiency in DSSCs. Therefore, our results reveal

**Table 2. Computed Vertical Excitation Energies ($E$), Oscillator Strengths ($f$), the Maximum Absorption Wavelength ($\lambda_{max}$), and the Dominant Configurations of Dimers in $CH_2Cl_2$ Solution**

| dimer | state | $E$ (eV) | $f$ | $\lambda_{max}$ (nm) | MO character | shift[a] |
|---|---|---|---|---|---|---|
| $(LS\text{-}1)_2$-A | $S_1$ | 2.42 | 0.155 | 512.8 | H-1→L (48.4%) | −0.17 |
| | $S_2$ | 2.55 | 1.013 | 486.8 | H→L (54.9%) | −0.04 |
| $(LS\text{-}1)_2$-B | $S_1$ | 2.48 | 0.094 | 500.4 | H-1→L (53.0%) | −0.11 |
| | $S_2$ | 2.65 | 2.197 | 468.2 | H→L (53.0%) | 0.06 |
| $(IQ_4)_2$-A | $S_1$ | 2.35 | 0.208 | 527.5 | H→L (63.4%) | −0.15 |
| | $S_2$ | 2.52 | 0.892 | 492.2 | H-1→L (62.1%) | 0.02 |
| $(IQ_4)_2$-B | $S_1$ | 2.20 | 0.171 | 564.7 | H→L (62.9%) | −0.30 |
| | $S_2$ | 2.30 | 1.179 | 539.3 | H-1→L (66.0%) | −0.20 |

[a]Shifts (eV) with respect to the corresponding monomer in $CH_2Cl_2$ solution.



DOI: 10.1021/acsami.5b06743
ACS Appl. Mater. Interfaces 2015, 7, 22504−22514

that the dye aggregates partly contribute to the observed absorption spectra.

As found in our recent work,[44] there is a close relationship between absorption spectra and dimer structure. Therefore, further investigations are focused on the dimeric configurations by detecting the variation of dihedral angles between different units from isolated to aggregated dyes. The selected dihedral angles are summarized in Tables S2−S3, and the sketches of the dihedral angles for $(LS\text{-}1)_2$ dimers and $(IQ_4)_2$ dimers are presented in Figure 3b. For LS-1 dimers, the variations of

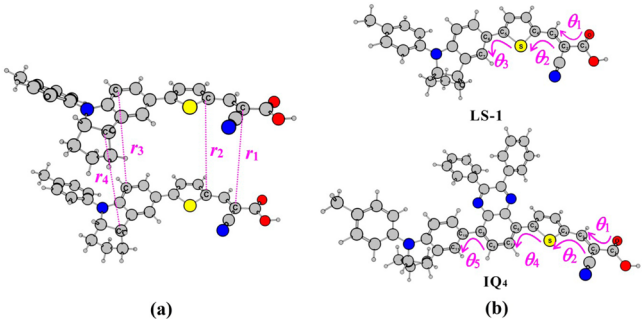


**Figure 3.** Schematic presentation of (a) intermolecular distances ($r_1$−$r_4$) between two individual dyes in a dimer ($r_1$ and $r_2$ for the distances between $\pi$ units; $r_3$ and $r_4$ for the distances between donor parts) and (b) dihedral angles ($\theta_1$−$\theta_5$) between different units of LS-1 and $IQ_4$.

dihedral angles of two adjacent indole and thiophene units ($\theta_3$ in Figure 3b) for different individual molecules in the dimeric configuration (the two dyes in a dimer labeled as mole1 and mole2) are contrary: $\theta_3$ increases from 14.6° in isolated LS-1 to −26.0 and 23.4° in $(LS\text{-}1)_2$-A-mole1 and $(LS\text{-}1)_2$-B-mole1, respectively, whereas $\theta_3$ in $(LS\text{-}1)_2$-mole2 reduces to −5.7 and −3.2° for $(LS\text{-}1)_2$-A-mole2 and for $(LS\text{-}1)_2$-B-mole2, respectively (Table S2). In $IQ_4$ dimers, $\theta_5$ (the dihedral angle between the indole and diphenylquinoxaline unit, see Figure 3), is −39.1, −48.4, and −35.7° for $IQ_4$, $(IQ_4)_2$-A-mole1 and $(IQ_4)_2$-A-mole2, respectively (Table S3). However, in $(IQ_4)_2$-B: $\theta_4$ (the dihedral angle between thiophene unit and diphenylquinoxaline unit) and $\theta_5$ are reduced when dimers form. $\theta_4$ is −30.7, −6.0, and −6.0°and $\theta_5$ is −39.1, −35.7, and −35.7° for the monomers of $IQ_4$, $(IQ_4)_2$-B-mole1, and $(IQ_4)_2$-B-mole2, respectively. As highlighted above, the absorption spectrum of $(IQ_4)_2$-B is red-shifted relative to isolated $IQ_4$. In contrast, the absorption spectra of the other dimers ($(LS\text{-}1)_2$-A, $(LS\text{-}1)_2$-B, and $(IQ_4)_2$-A) are roughly equal to those of the monomers. These results suggest that the steric hindrance induced by the diphenylquinoxaline unit in $IQ_4$ leads to a more planar molecular structure as evidenced by decreased dihedral angles $\theta_4$ and $\theta_5$ in $(IQ_4)_2$-B. This in turn is responsible for the redshift in absorption spectra.

**3.2. Structures and Optical Properties on $TiO_2$.** It is known that organic dyes are more inclined to adsorb on $TiO_2$ in a bridged bidentate mode than in the monodentate mode.[65,66] We adopt the bidentate mode by linking the carboxylate group to five-coordinated titanium atoms of the $TiO_2$ surface. The optimized structures of dye monomers on $TiO_2$ are shown in Figure S2. It has been known one of the key parameters controlling charge transfer at dye/$TiO_2$ interface is the spatial distance from the cation center of the dye to the $TiO_2$ surface.[67,68] The shorter the distance between the dye cation HOMO and the semiconductor surface, the faster the charge recombination in DSSCs.[67,68] Following the methodology developed by Durrant and co-workers, the dye-cation/$TiO_2$ spatial separation $r$ was determined by calculating the geometric distance between the carbon atom of the carboxylic group and each atom of the dye and by weighting this value with the square of the percentage contribution of the atom to the HOMO orbital.[67] As shown in Figure 4, the spatial distance

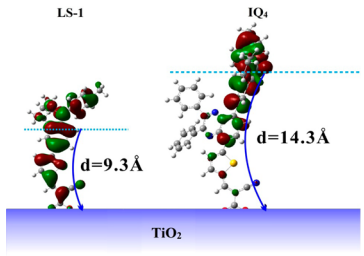


**Figure 4.** Distances between the hole of dye cation and $TiO_2$ surface for LS-1 and $IQ_4$.

of $IQ_4$ (14.3 Å) is much longer than that of LS-1 (9.3 Å), implying less charge recombination possibility in the $IQ_4$-based device via the through-bond transfer path.

Following our recent work,[44] four possible adsorption positions for dye aggregates on the $TiO_2$ surface are chosen (Figure 5). Considering steric hindrance and asymmetry with

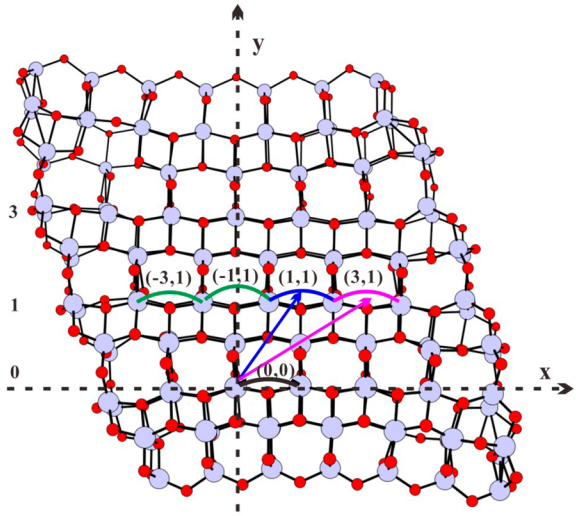


**Figure 5.** Aggregation configurations of dimers on the (101) $TiO_2$ surface (the *xy* plane). The first molecule in dimers is fixed at (0, 0). Four possible absorption sites of the second molecule have been considered, where the energetically most favorable sites for LS-1 and $IQ_4$ are highlighted with arrows and marked in blue and pink, respectively.

respect to the molecular axis, the molecules situated on the second row of the $TiO_2$ surface adopt two possible orientations relative to the molecular axis as in $CH_2Cl_2$ solution. The adsorption positions in the second row are labeled as (−1,1)-A, (1,1)-A, (−3,1)-A, (3,1)-A, (−1,1)-B, (1,1)-B, and (3,1)-B.

To gain more insight into the possible interactions occurring between dye aggregates on the $TiO_2$ surface, we carried out MD simulations within the DFTB framework for all dye−surface complexes mentioned above. The total electronic energy evolutions of the system as a function of the simulation time are documented in Figures S3 and S4, which illustrate that


DOI: 10.1021/acsami.5b06743
ACS Appl. Mater. Interfaces 2015, 7, 22504−22514

the system of dye aggregates on $TiO_2$ has reached thermal equilibrium roughly within 2 ps. From the dynamics simulation, we extracted the lowest energy structure of each trajectory as the starting geometry for subsequent structure optimization. All the optimized structures are displayed in Figures S3 and S4. In a next step, the interaction energies between the two aggregated dyes on $TiO_2$ were computed at the B3LYP level and are shown in Table 3. We can see that the smallest interaction energy for $(LS\text{-}1)_2$ dimers occurs for the (1,1) configuration, where the two molecules align along the $y$ direction (Figure 5, in blue) with the $\pi$ systems almost perfectly stacked. However, the lowest-energy configuration for $(IQ_4)_2$ dimers is at (3,1)-B, where one $IQ_4$ molecule shifts to the right along the second row and the two dyes orientate oppositely, which disrupts the perfect $\pi-\pi$ stacking (Figure 5, in pink). Clearly, the steric hindrance arising from the added diphenylquinoxaline units on the molecular skeleton results in a less stacked dimeric configuration of $IQ_4$ on $TiO_2$ compared with that of LS-1.

**Table 3. Interaction Energies (eV) at B3LYP/6-31G(d, p) Level for $(LS\text{-}1)_2$ and $(IQ_4)_2$ on $TiO_2$**

| dimer[a] | $(LS\text{-}1)_2$ | $(IQ_4)_2$ |
|---|---|---|
| (−1,1)-A | −0.62 | −1.53 |
| (1,1)-A | −0.83 | −1.82 |
| (−3,1)-A | −0.49 | −0.64 |
| (3,1)-A | −0.56 | −1.07 |
| (−1,1)-B | −0.46 | −0.68 |
| (1,1)-B | −0.69 | −1.85 |
| (3,1)-B | −0.41 | −1.93 |

[a]The calculations have been carried out on the protonated dyes in $CH_2Cl_2$ solution.

The optical properties of the aggregated dyes on $TiO_2$ (Figure 2c,d) were obtained by utilizing the same computational procedure as that for the dyes in solution but removing the $(TiO_2)_{124}$ cluster. The critical data about the absorption spectra of dyes adsorbed on $TiO_2$ are collected in Table 4. Similar to the dimers in solution, the $S_0 \rightarrow S_1$ transition of $(1,1)$-$(LS\text{-}1)_2$-A is at a longer wavelength (523 nm), but it is not visible on the spectrum because of the small oscillator strength (0.084). The absorption maxima of dimers on $TiO_2$ are located at 2.72 and 2.42 eV for $(1,1)$-$(LS\text{-}1)_2$-A and $(3,1)$-$(IQ_4)_2$-B, respectively, which are in good agreement with the experimental trend (2.81 and 2.48 eV).[27,32] The slight blueshifts of dimer absorption maxima compared to those of the monomer are ascribed to the variation of the dye configurations when aggregated on the $TiO_2$ surface. As shown in Table S2, the dihedral angle $\theta_3$ of LS-1 (defined in Figure 3 b) grows from 26.8° in LS-1 on $(TiO_2)_{124}$ to −32.5° in $(1,1)$-$(LS\text{-}1)_2$-A-mole1 and decreases to −14.7° in $(1,1)$-$(LS\text{-}1)_2$-A-mole2. Similarly, the dihedral angle $\theta_4$ of $IQ_4$ is −10.3, −3.4, and −16.6° for isolated $IQ_4$ on $(TiO_2)_{124}$, $(3,1)$-$(IQ_4)_2$-B-mole1, and $(3,1)$-$(IQ_4)_2$-B-mole2, respectively (Table S3). Besides that, the difference of the dihedral angle $\theta_4$ from monomer to dimer is smaller when $IQ_4$ aggregates on $TiO_2$ compared to the value in solution. The angle $\theta_5$ is −46.7, −44.4, and −36.5° for $(3,1)$-$(IQ_4)_2$-B, $(3,1)$-$(IQ_4)_2$-B-mole1, and $(3,1)$-$(IQ_4)_2$-B-mole2, respectively. This shows that the adsorption of the dyes on $TiO_2$ leads to significant structural changes of the chromophores.

**3.3. Dynamic Simulation.** To further investigate the aggregation effects, we have carried out molecular dynamic simulations within the DFTB framework starting from the two lowest-energy configurations, $(1,1)$-$(LS\text{-}1)_2$-A and $(3,1)$-$(IQ_4)_2$-B. The influence of the diphenylquinoxaline unit on the aggregation behavior is analyzed below from a time-dependent perspective.

The evolutions of intermolecular distances as a function of simulation time are inspected for the different dimers on $(TiO_2)_{124}$ in Figure 6. The shown parameters for $(1,1)$-$(LS\text{-}1)_2$-A and $(3,1)$-$(IQ_4)_2$-B are defined in Figure 3a. Four distances $(r_1-r_4)$ are chosen to evaluate the separations between intermolecular $\pi$ units or electron donors, where $r_1$ and $r_2$ are

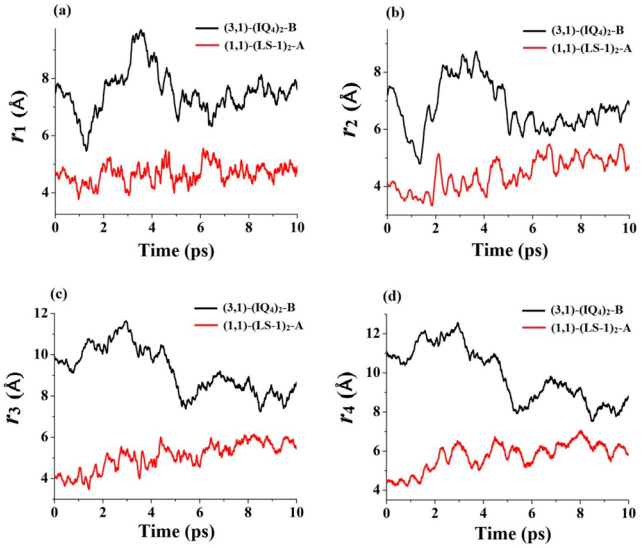


**Figure 6.** Time profiles of intermolecular distances (a) $r_1$ ,(b) $r_2$, (c) $r_3$, and (d) $r_4$ throughout 10 ps of molecular dynamics for $(1,1)$-$(LS\text{-}1)_2$-A (in red) and $(3,1)$-$(IQ_4)_2$-B (in black). (See Figure 3 for the definitions of $r_1-r_4$.)

**Table 4. Computed Vertical Excitation Energies ($E$), Oscillator Strengths ($f$), the Maximum Absorption Wavelength ($\lambda_{max}$), and the Dominant Configurations for the Monomers and Dimers of LS-1 and $IQ_4$ Absorbed on $TiO_2$**

| species | state | $E$ (eV) | $\lambda_{max}$ (nm) | $f$ | MO character | shift[a] |
|---|---|---|---|---|---|---|
| LS-1 on $TiO_2$ | $S_1$ | 2.70 | 459 | 1.095 | H→L (68.3%) | 0.00 |
| $IQ_4$ on $TiO_2$ | $S_1$ | 2.36 | 525 | 0.964 | H→L (65.5%) | 0.00 |
| $(1,1)$-$(LS\text{-}1)_2$-A | $S_1$ | 2.46 | 505 | 0.084 | H→L (66.2%) | −0.24 |
| | $S_2$ | 2.72 | 456 | 1.862 | H→L+1 (59.1%) | 0.02 |
| $(3,1)$- $(IQ_4)_2$-B | $S_1$ | 2.37 | 523 | 0.244 | H-1→L (54.1%) | −0.13 |
| | $S_2$ | 2.42 | 512 | 1.533 | H→L+1 (57.6%) | 0.06 |

[a]With respect to the corresponding monomer on $TiO_2$.



DOI: 10.1021/acsami.5b06743
ACS Appl. Mater. Interfaces 2015, 7, 22504−22514

for the intermolecular distances of $\pi$ units and $r_3$ and $r_4$ represent the intermolecular distances of donor parts.

Initially, there are noticeably longer average intermolecular distances in (3,1)-$(IQ_4)_2$-B than those in (1,1)-$(LS\text{-}1)_2$-A. The average values of $r_1-r_4$ in (3,1)-$(IQ_4)_2$-B are 7.5, 6.7, 9.0, and 9.6 Å, respectively, whereas they are 4.7, 4.5, 5.1, and 5.8 Å in (1,1)-$(LS\text{-}1)_2$-A, respectively. This suggests that the steric hindrance induced by the diphenlyquinoxaline unit in $IQ_4$ efficiently increases the intermolecular distance of the stacked dyes on $TiO_2$. Moreover, in Figure 6 we can see wide fluctuations appearing in the trajectories of (3,1)-$(IQ_4)_2$-B, where the peak values of $r_1-r_4$ are 9.7, 8.8, 11.6, and 12.6 Å, respectively, at around 3.5 ps. The structural fluctuations of (3,1)-$(IQ_4)_2$-B were further explored by analyzing the evolution of the dihedral $\theta$ illustrated in Figure 7. The dihedral $\theta$ represents the angle of the carboxylate group of the dye and the two binding five-coordinated Ti atoms of the $TiO_2$ surface. Note that the two dyes in the dimer behave similarly during the dynamics simulation, so the discussion below focuses on the dihedral angle in one dye only. The $\theta$ value varies greatly for (3,1)-$(IQ_4)_2$-B, with a peak at 3 ps and gradually increases from 7 to 10 ps (from −5 to 98°). Interestingly, the dye−$TiO_2$ binding mode changes between the bidentate bridging form (0−2.5 and 4.5−6.5 ps) and the monodentate pattern (3 and 8−10 ps) along the dynamics. Meanwhile, the trajectory of (1,1)-$(LS\text{-}1)_2$-A is relatively smooth during the whole simulation, where the binding mode keeps the bidentate form with the dihedral $\theta$ fluctuating between −5 and 5° (Figure 7). The wider fluctuations in (3,1)-$(IQ_4)_2$-B are ascribed to the weak $\pi-\pi$ stacking interaction induced by the steric hindrance in $IQ_4$.

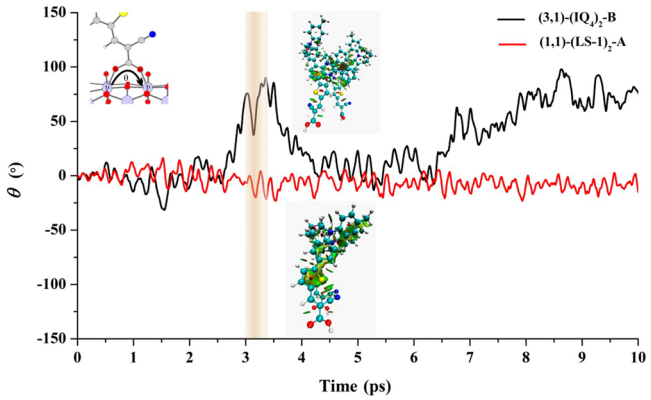


**Figure 7.** Molecular dynamics trajectory of the dihedrals for (1,1)-$(LS\text{-}1)_2$-A (in red) and (3,1)-$(IQ_4)_2$-B (in black). Insets: Dihedral angle $\theta$ between the carboxylate group of the dye and the two binding five-coordinated titanium atoms of the $TiO_2$ surface. Reduced density gradient (RDG) isosurfaces (isovalue of 0.6) for the snapshot at 3 ps are also shown for (1,1)-$(LS\text{-}1)_2$-A (bottom) and (3,1)-$(IQ_4)_2$-B (top). The weak, the strong attractive, and the strong repulsive interactions are depicted in green, blue, and red, respectively.

To visualize the noncovalent interactions in the dye aggregates,[69,70] we have extracted a snapshot at 3 ps and used the method developed by Yang and co-workers to calculate the reduced density gradient (RDG). This RDG method is capable of describing the intermolecular and intramolecular noncovalent interactions in real space on the basis of the electron density and its second Hessian eigenvalue.[69] The inset of Figure 7 displays the obtained RDG isosurfaces, where different types (attractive/repulsive) and strength of noncovalent interactions are depicted by various colors. Clearly, the region of $\pi-\pi$ stacking interaction (quantified by the depicted isosurface) for (3,1)-$(IQ_4)_2$-B is smaller than that of (1,1)-$(LS\text{-}1)_2$-A, indicating weaker intermolecular interaction between dimers in (3,1)-$(IQ_4)_2$-B.

Besides that, quite diverse surface coverage modes for the two dyes are found in the time-dependent simulations. We examine the evolution of the distance from a carbon atom in the thiophene unit of the dye to a surface Ti atom $r_{C-Ti}$. It is clearly shown in Figure 8, that dyes in (1,1)-$(LS\text{-}1)_2$-A favor bending toward the $TiO_2$ surface, with $r_{C-Ti}$ decreasing from 7.1 to 3.0 Å during the simulation. Three snapshots of (1,1)-$(LS\text{-}1)_2$-A extracted at 1, 5, and 10 ps illustrate this behavior (inset of Figure 8). As for the tilt angle, one LS-1 molecule in (1,1)-$(LS\text{-}1)_2$-A has an inclination with respect to $TiO_2$ surface of about 108, 66, and 57° at 1, 5, and 10 ps, respectively. In contrast, the dyes in (3,1)-$(IQ_4)_2$-B remain almost perpendicular to the $TiO_2$ surface, which can be identified from the trajectory of $r_{C-Ti}$ for (3,1)-$(IQ_4)_2$-B ($r_{C-Ti} \approx 7.4$ Å) and the corresponding snapshots. Regarding the tilt angle, it is 113, 82,

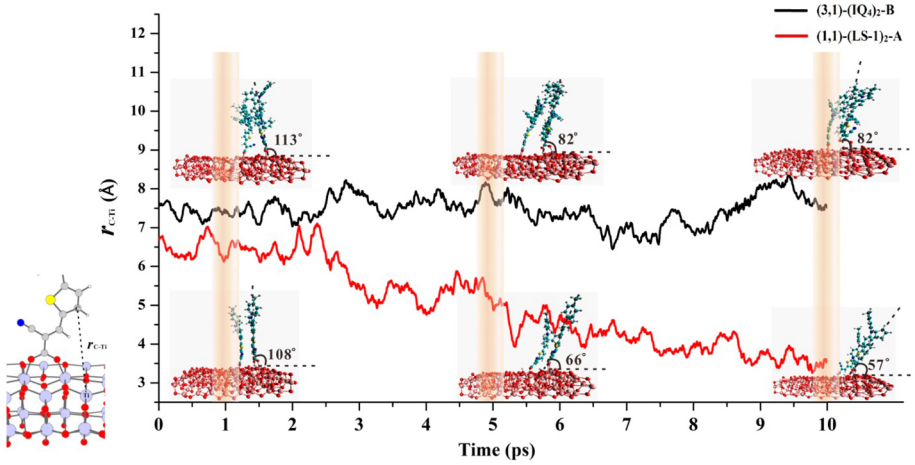


**Figure 8.** Evolutions of $r_{C-Ti}$ distance as a function of time for (1,1)-$(LS\text{-}1)_2$-A (in red) and (3,1)-$(IQ_4)_2$-B (in black) in the dynamics. $r_{C-Ti}$ represents the distance from one carbon atom of thiophene unit to the nearest Ti atom of the $TiO_2$ surface. (See the diagram on the left.) Inset: three snapshots of patterns at 1, 5, and 10 ps, where the tilt angles of the dye to the $TiO_2$ surface are shown.


DOI: 10.1021/acsami.5b06743
ACS Appl. Mater. Interfaces 2015, 7, 22504−22514

and 82° for one $IQ_4$ in (3,1)-$(IQ_4)_2$-B at 1, 5, and 10 ps, respectively. As a result, a higher probability of recombination between oxidized dyes and $TiO_2$-injected electrons exists in LS-1 compared to that in $IQ_4$. These trends are in line with experimental observations, where the electron lifetime of LS-1 (2.9 ms) is smaller than that of $IQ_4$ (4.7 ms).[27,32] Therefore, the diphenylquinoxaline unit incorporated into $IQ_4$ can effectively keep the dyes perpendicular to the $TiO_2$ surface, thus reducing unwanted through-space electron recombination that is more serious in the case of LS-1.

**3.4. Intermolecular Electronic Coupling.** Because it is known that small intermolecular electronic coupling $|V|$ is responsible for weak intermolecular charge-transfer character and significant improvement in $J_{SC}$ and $V_{OC}$ of dyes in DSSCs,[44] we calculate this parameter to further assess the aggregation of dyes. The computed intermolecular electronic coupling values in $CH_2Cl_2$ solution are listed in Table 5. For

**Table 5. Intermolecular Electronic Couplings (eV) of LS-1 and $IQ_4$ Dimers in Solution**

| | intermolecular electronic coupling $\|V\|$ | |
|---|---|---|
| dimer | ESID method | direct method |
| $(LS\text{-}1)_2$-A | 0.051 | 0.033 |
| $(LS\text{-}1)_2$-B | 0.014 | 0.006 |
| $(IQ_4)_2$-A | 0.027 | 0.022 |
| $(IQ_4)_2$-B | 0.004 | 0.005 |

$(IQ_4)_2$-B, the coupling is 0.004 eV by the EDIS method and 0.005 eV according to the direct method, which is smaller than the values of $(LS\text{-}1)_2$-A (0.051 and 0.033 eV) and $(LS\text{-}1)_2$-B (0.014 and 0.006 eV). Regarding $(IQ_4)_2$-A, the couplings are larger than those of $(IQ_4)_2$-B and $(LS\text{-}1)_2$-B but smaller compared with those of $(LS\text{-}1)_2$-A. This illustrates that the intermolecular interactions in $(LS\text{-}1)_2$ dimers are generally stronger than those in $(IQ_4)_2$ dimers and that the face-to-face stacking pattern (form A) induces more compact aggregates with respect to the face-to-back ones (form B) in solution.

To evaluate the intermolecular electronic coupling for the aggregated dyes on $TiO_2$, we extracted 10 snapshots every picosecond at random along the dynamics simulation and computed the corresponding dye−dye intermolecular couplings by the direct method. As shown in Figure 9, the

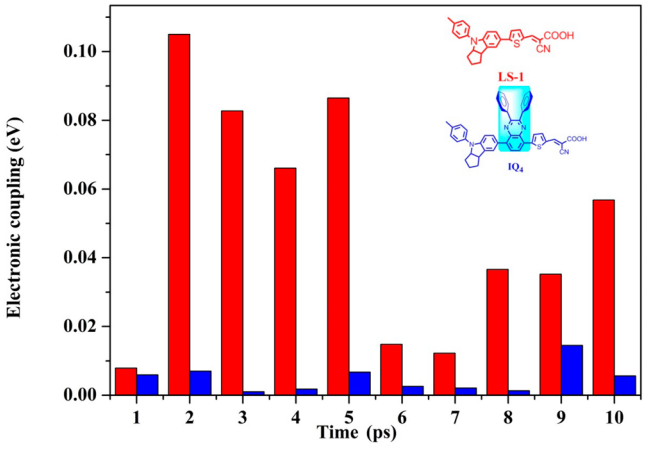


**Figure 9.** Intermolecular electronic couplings of 10 selected snapshots in dynamics. (1,1)-$(LS\text{-}1)_2$-A, red, and (3,1)-$(IQ_4)_2$-B, blue.

couplings of (3,1)-$(IQ_4)_2$-B are clearly lower than those of (1,1)-$(LS\text{-}1)_2$-A. The average value of 0.039 eV in (1,1)-$(LS\text{-}1)_2$-A is approximately 10 times larger than that of 0.004 eV in (3,1)-$(IQ_4)_2$-B. It is remarkable that the computed coupling values for $(IQ_4)_2$ dimers, whether in solution or on $TiO_2$, are smaller than those of $(LS\text{-}1)_2$ dimers regardless of the employed method and simulation time, revealing a strong self-anti-aggregation capability by introducing a diphenylquinoxaline unit on the dye skeleton. Moreover, as shown in Figure 10, the $S_1$ state of (3,1)-$(IQ_4)_2$-B, which mainly arises

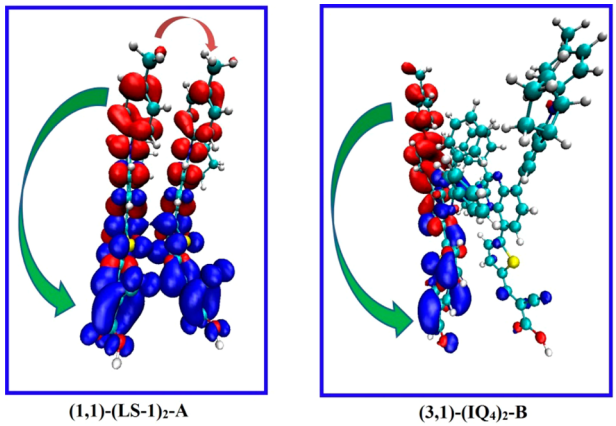


**Figure 10.** Molecular orbital diagrams of (1,1)-$(LS\text{-}1)_2$-A and (3,1)-$(IQ_4)_2$-B on $TiO_2$ ($(TiO_2)_{124}$ cluster not shown). Red and blue correspond to HOMO electronic density and LUMO electronic density, respectively. Arrows represent the charge transfer direction.

from an intramolecular HOMO → LUMO transition, is localized on one molecule of the dimer as shown in Figure 10. In contrast, for (1,1)-$(LS\text{-}1)_2$-A, the HOMO and LUMO are delocalized over the dimer and the intermolecular charge-transfer character is evident. This confirms that $IQ_4$ has the capability of self-anti-aggregation accompanied by weak intermolecular electronic coupling and significant intramolecular charge transfer character upon excitation.

It is furthermore noted that the intermolecular electronic coupling and charge-transfer characters are correlated with the intermolecular distances of the electron donors in dimers. The longer the distance between donors (Table S4 and Figure 6, in $(IQ_4)_2$-B, $r_3$ = 7.7 Å and $r_4$ = 12.2 Å; in (3,1)-$(IQ_4)_2$-B, averaged $r_3$ = 9.0 Å and $r_4$ = 9.6 Å), the smaller the couplings (Table 5 and Figure 9, for $(IQ_4)_2$-B, $|V|$ = 0.005 eV; in (3,1)-$(IQ_4)_2$-B, averaged $|V|$ = 0.004 eV) and vice versa (in $(LS\text{-}1)_2$-A $r_3$ = 3.9 Å, $r_4$ = 4.7 Å, and $|V|$ = 0.033 eV; in (1,1)-$(LS\text{-}1)_2$-A, averaged $r_3$ = 5.1 Å, $r_4$ = 5.8 Å, and $|V|$ = 0.039 eV). The weaker intermolecular electronic couplings for $IQ_4$ in $CH_2Cl_2$ solution and on $TiO_2$, which are induced by steric hindrance due to the additional diphenylquinoxaline unit, can therefore explain the significant improvement of conversion efficiency for $IQ_4$-based DSSCs compared to that of LS-1-based devices under the same conditions.[27,32]

## 4. CONCLUSIONS

In this work, computational investigations have been carried out to understand the influence of dye aggregations on the photovoltaic performance of DSSCs by comparing the optical properties and dye−dye intermolecular electronic couplings of two sensitizers (LS-1 and $IQ_4$) differing by the addition of a diphenylquinoxaline antiaggregation unit within $IQ_4$. Various


DOI: 10.1021/acsami.5b06743
ACS Appl. Mater. Interfaces 2015, 7, 22504−22514

dimeric configurations in solution and on a $TiO_2$ surface have been considered. Owing to the steric hindrance effect of the diphenylquinoxaline group on the molecular skeleton, the preferred dimeric arrangements of $IQ_4$ show a disrupted $\pi-\pi$ stacking both in $CH_2Cl_2$ solution and on the $TiO_2$ surface. Vertical excitation energies reveal that the absorption spectra observed experimentally arise from not only the dye monomers but also the dye aggregates in various patterns. Dynamics simulations show that in contrast to the LS-1 dimer the two dyes in the $IQ_4$ dimer are well-separated and stand almost perpendicular on the $TiO_2$ surface with bidentate and monodentate binding forms alternating. This implies less lateral charge transfer between adjacent dyes and a smaller recombination probability of the injected electrons in $TiO_2$ with the oxidized dyes. The average dye−dye intermolecular electronic coupling in the $IQ_4$ dimer along the dynamics trajectory is only around 10% of that in the LS-1 dimer, which nicely evidences the significant self-anti-aggregation capability of the diphenylquinoxaline unit in $IQ_4$. This further results in weaker intermolecular charge-transfer character and higher photovoltaic efficiency.

Our work sheds new light on aggregation effects governing the optical properties, recombination processes, and intermolecular charge transfer occurring in DSSCs, which may assist the molecular engineering of more efficient anti-aggregation sensitizers and deeper understanding of the electron transfer dynamics in solar cells. It has been well-known that the power conversion efficiency of DSSC is determined by many associated factors. Thereby, it should be stressed that the assessment of only one feature (such as aggregation effect) is inadequate for the evaluation of a dye in the complicated DSSC system whereas the perfect balance in various aspects is a prerequisite for the rational design of efficient sensitizers.

## ■ ASSOCIATED CONTENT

### Supporting Information

The Supporting Information is available free of charge on the ACS Publications website at DOI: 10.1021/acsami.5b06743.

Detailed description of aggregations pattern, optimized structures of dyes on $TiO_2$, interaction energies of dimers in solution, and selected geometric parameters of isolated dyes and dimers in solution and on $TiO_2$. (PDF)

## ■ AUTHOR INFORMATION

### Corresponding Author

*E-mail: liquansong@bit.edu.cn.

### Notes

The authors declare no competing financial interest.

## ■ ACKNOWLEDGMENTS

We gratefully acknowledge the financial support of the Major State Basic Research Development Programs of China (2011CBA00701) and the National Natural Science Foundation of China (21303007, 21473010).

## ■ REFERENCES

(1) O'Regan, B.; Gratzel, M. A Low-Cost, High-Efficiency Solar Cell Based on Dye-Sensitized Colloidal $TiO_2$ Films. *Nature* **1991**, *353*, 737−740.

(2) Nazeeruddin, M. K.; De Angelis, F.; Fantacci, S.; Selloni, A.; Viscardi, G.; Liska, P.; Ito, S.; Takeru, B.; Grätzel, M. Combined Experimental and DFT-TDDFT Computational Study of Photoelectrochemical Cell Ruthenium Sensitizers. *J. Am. Chem. Soc.* **2005**, *127*, 16835−16847.

(3) Grätzel, M. Recent Advances in Sensitized Mesoscopic Solar Cells. *Acc. Chem. Res.* **2009**, *42*, 1788−1798.

(4) Mathew, S.; Yella, A.; Gao, P.; Humphry-Baker, R.; Curchod, B. F. E.; Ashari-Astani, N.; Tavernelli, I.; Rothlisberger, U.; Nazeeruddin, M. K.; Grätzel, M. Dye-Sensitized Solar Cells with 13% Efficiency Achieved through the Molecular Engineering of Porphyrin Sensitizers. *Nat. Chem.* **2014**, *6*, 242−247.

(5) Mishra, A.; Fischer, M. K. R.; Bäuerle, P. Metal-Free Organic Dyes for Dye-Sensitized Solar Cells: From Structure: Property Relationships to Design Rules. *Angew. Chem., Int. Ed.* **2009**, *48*, 2474−2499.

(6) Kim, S.; Lee, J. K.; Kang, S. O.; Ko, J.; Yum, J. H.; Fantacci, S.; De Angelis, F.; Di Censo, D.; Nazeeruddin, M. K.; Grätzel, M. Molecular Engineering of Organic Sensitizers for Solar Cell Applications. *J. Am. Chem. Soc.* **2006**, *128*, 16701−16707.

(7) Jiao, Y.; Zhang, F.; Grätzel, M.; Meng, S. Structure-Property Relations in All-Organic Dye-Sensitized Solar Cells. *Adv. Funct. Mater.* **2013**, *23*, 424−429.

(8) Hagberg, D. P.; Edvinsson, T.; Marinado, T.; Boschloo, G.; Hagfeldt, A.; Sun, L. A Novel Organic Chromophore for Dye-Sensitized Nanostructured Solar Cells. *Chem. Commun.* **2006**, 2245−2247.

(9) Yao, Z.; Zhang, M.; Wu, H.; Yang, L.; Li, R.; Wang, P. Donor/Acceptor Indenoperylene Dye for Highly Efficient Organic Dye-Sensitized Solar Cells. *J. Am. Chem. Soc.* **2015**, *137*, 3799−3802.

(10) Nazeeruddin, M. K.; Kay, A.; Rodicio, I.; Humphrybaker, R.; Mueller, E.; Liska, P.; Vlachopoulos, N.; Graetzel, M. Conversion of Light to Electricity by Cis-x2bis(2,2′-Bipyridyl-4,4′-Dicarboxylate)-Ruthenium(II) Charge-Transfer Sensitizers (X = $Cl^-$, $Br^-$, $I^-$, $CN^-$, and $SCN^-$) on Nanocrystalline $TiO_2$ Electrodes. *J. Am. Chem. Soc.* **1993**, *115*, 6382−6390.

(11) Nazeeruddin, M. K.; Pechy, P.; Renouard, T.; Zakeeruddin, S. M.; Humphry-Baker, R.; Comte, P.; Liska, P.; Cevey, L.; Costa, E.; Shklover, V.; Spiccia, L.; Deacon, G. B.; Bignozzi, C. A.; Grätzel, M. Engineering of Efficient Panchromatic Sensitizers for Nanocrystalline $TiO_2$-Based Solar Cells. *J. Am. Chem. Soc.* **2001**, *123*, 1613−1624.

(12) Sayama, K.; Tsukagoshi, S.; Hara, K.; Ohga, Y.; Shinpou, A.; Abe, Y.; Suga, S.; Arakawa, H. Photoelectrochemical Properties of J Aggregates of Benzothiazole Merocyanine Dyes on a Nanostructured $TiO_2$ Film. *J. Phys. Chem. B* **2002**, *106*, 1363−1371.

(13) Kawasaki, M.; Aoyama, S. High Efficiency Photocurrent Generation by Two-Dimensional Mixed J-Aggregates of Cyanine Dyes. *Chem. Commun.* **2004**, 988−989.

(14) Wang, Z.-S.; Cui, Y.; Dan-oh, Y.; Kasada, C.; Shinpo, A.; Hara, K. Thiophene-Functionalized Coumarin Dye for Efficient Dye-Sensitized Solar Cells: Electron Lifetime Improved by Coadsorption of Deoxycholic Acid. *J. Phys. Chem. C* **2007**, *111*, 7224−7230.

(15) Tatay, S.; Haque, S. A.; O'Regan, B.; Durrant, J. R.; Verhees, W. J. H.; Kroon, J. M.; Vidal-Ferran, A.; Gaviña, P.; Palomares, E. Kinetic Competition in Liquid Electrolyte and Solid-State Cyanine Dye Sensitized Solar Cells. *J. Mater. Chem.* **2007**, *17*, 3037−3044.

(16) Wang, M.; Li, X.; Lin, H.; Pechy, P.; Zakeeruddin, S. M.; Gratzel, M. Passivation of Nanocrystalline $TiO_2$ Junctions by Surface Adsorbed Phosphinate Amphiphiles Enhances the Photovoltaic Performance of Dye Sensitized Solar Cells. *Dalton. Trans.* **2009**, 10015−10020.

(17) Han, L.; Islam, A.; Chen, H.; Malapaka, C.; Chiranjeevi, B.; Zhang, S.; Yang, X.; Yanagida, M. High-Efficiency Dye-Sensitized Solar Cell with a Novel Co-Adsorbent. *Energy Environ. Sci.* **2012**, *5*, 6057−6060.

(18) Ning, Z.; Zhang, Q.; Wu, W.; Pei, H.; Liu, B.; Tian, H. Starburst Triarylamine Based Dyes for Efficient Dye-Sensitized Solar Cells. *J. Org. Chem.* **2008**, *73*, 3791−3797.

(19) Liu, B.; Liu, Q.; You, D.; Li, X.; Naruta, Y.; Zhu, W. Molecular Engineering of Indoline Based Organic Sensitizers for Highly Efficient Dye-Sensitized Solar Cells. *J. Mater. Chem.* **2012**, *22*, 13348−13356.



DOI: 10.1021/acsami.5b06743
*ACS Appl. Mater. Interfaces* 2015, 7, 22504−22514

(20) Zhang, G.; Bala, H.; Cheng, Y.; Shi, D.; Lv, X.; Yu, Q.; Wang, P. High Efficiency and Stable Dye-Sensitized Solar Cells with an Organic Chromophore Featuring a Binary π-Conjugated Spacer. *Chem. Commun.* **2009**, 2198−2200.
(21) Li, W.; Wu, Y.; Li, X.; Xie, Y.; Zhu, W. Absorption and Photovoltaic Properties of Organic Solar Cell Sensitizers Containing Fluorene Unit as Conjunction Bridge. *Energy Environ. Sci.* **2011**, *4*, 1830−1837.
(22) Ito, S.; Miura, H.; Uchida, S.; Takata, M.; Sumioka, K.; Liska, P.; Comte, P.; Pechy, P.; Grätzel, M. High-Conversion-Efficiency Organic Dye-Sensitized Solar Cells with a Novel Indoline Dye. *Chem. Commun.* **2008**, 5194−5196.
(23) Jørgensen, M.; Norrman, K.; Gevorgyan, S. A.; Tromholt, T.; Andreasen, B.; Krebs, F. C. Stability of Polymer Solar Cells. *Adv. Mater.* **2012**, *24*, 580−612.
(24) Qu, S.; Qin, C.; Islam, A.; Wu, Y.; Zhu, W.; Hua, J.; Tian, H.; Han, L. A Novel D-A-π-A Organic Sensitizer Containing a Diketopyrrolopyrrole Unit with a Branched Alkyl Chain for Highly Efficient and Stable Dye-Sensitized Solar Cells. *Chem. Commun.* **2012**, *48*, 6972−6974.
(25) Zhu, W.-H.; Wu, Y.-Z.; Wang, S.-T.; Li, W.-Q.; Li, X.; Chen, J.; Wang, Z.-S.; Tian, H. Organic D-A-π-A Solar Cell Sensitizers with Improved Stability and Spectral Response. *Adv. Funct. Mater.* **2011**, *21*, 756−763.
(26) Wu, Y.; Zhang, X.; Li, W.-Q.; Wang, Z.-S.; Tian, H.; Zhu, W. Hexylthiophene-Featured D-A-π-A Structural Indoline Chromophores for Coadsorbent-Free and Panchromatic Dye-Sensitized Solar Cells. *Adv. Energy Mater.* **2012**, *2*, 149−156.
(27) Li, W.; Wu, Y.; Zhang, Q.; Tian, H.; Zhu, W. D-A-π-A Featured Sensitizers Bearing Phthalimide and Benzotriazole as Auxiliary Acceptor: Effect on Absorption and Charge Recombination Dynamics in Dye-Sensitized Solar Cells. *ACS Appl. Mater. Interfaces* **2012**, *4*, 1822−1830.
(28) Cui, Y.; Wu, Y.; Lu, X.; Zhang, X.; Zhou, G.; Miapeh, F. B.; Zhu, W.; Wang, Z.-S. Incorporating Benzotriazole Moiety to Construct D-A-π-A Organic Sensitizers for Solar Cells: Significant Enhancement of Open-Circuit Photovoltage with Long Alkyl Group. *Chem. Mater.* **2011**, *23*, 4394−4401.
(29) Pei, K.; Wu, Y.; Wu, W.; Zhang, Q.; Chen, B.; Tian, H.; Zhu, W. Constructing Organic D-A-π-A-Featured Sensitizers with a Quinoxaline Unit for High-Efficiency Solar Cells: The Effect of an Auxiliary Acceptor on the Absorption and the Energy Level Alignment. *Chem. - Eur. J.* **2012**, *18*, 8190−8200.
(30) Shi, J.; Chen, J.; Chai, Z.; Wang, H.; Tang, R.; Fan, K.; Wu, M.; Han, H.; Qin, J.; Peng, T.; Li, Q.; Li, Z. High Performance Organic Sensitizers Based on 11,12-Bis(Hexyloxy) Dibenzo [*a*,*c*] Phenazine for Dye-Sensitized Solar Cells. *J. Mater. Chem.* **2012**, *22*, 18830−18838.
(31) Lu, X.; Feng, Q.; Lan, T.; Zhou, G.; Wang, Z.-S. Molecular Engineering of Quinoxaline-Based Organic Sensitizers for Highly Efficient and Stable Dye-Sensitized Solar Cells. *Chem. Mater.* **2012**, *24*, 3179−3187.
(32) Pei, K.; Wu, Y.; Islam, A.; Zhang, Q.; Han, L.; Tian, H.; Zhu, W. Constructing High-Efficiency D-A-π-A-Featured Solar Cell Sensitizers: A Promising Building Block of 2,3-Diphenylquinoxaline for Anti-aggregation and Photostability. *ACS Appl. Mater. Interfaces* **2013**, *5*, 4986−4995.
(33) Wu, Y.; Zhu, W. H.; Zakeeruddin, S. M.; Gratzel, M. Insight into D-A-π-A Structured Sensitizers: A Promising Route to Highly Efficient and Stable Dye-Sensitized Solar Cells. *ACS Appl. Mater. Interfaces* **2015**, *7*, 9307−9318.
(34) Pastore, M.; De Angelis, F. Aggregation of Organic Dyes on $TiO_2$ in Dye-Sensitized Solar Cells Models: An Ab Initio Investigation. *ACS Nano* **2010**, *4*, 556−562.
(35) Agrawal, S.; Pastore, M.; Marotta, G.; Reddy, M. A.; Chandrasekharam, M.; De Angelis, F. Optical Properties and Aggregation of Phenothiazine-Based Dye-Sensitizers for Solar Cells Applications: A Combined Experimental and Computational Investigation. *J. Phys. Chem. C* **2013**, *117*, 9613−9622.
(36) Pastore, M.; De Angelis, F. Computational Modeling of Stark Effects in Organic Dye-Sensitized $TiO_2$ Heterointerfaces. *J. Phys. Chem. Lett.* **2011**, *2*, 1261−1267.
(37) Pastore, M.; De Angelis, F. Intermolecular Interactions in Dye-Sensitized Solar Cells: A Computational Modeling Perspective. *J. Phys. Chem. Lett.* **2013**, *4*, 956−974.
(38) Marotta, G.; Reddy, M. A.; Singh, S. P.; Islam, A.; Han, L.; De Angelis, F.; Pastore, M.; Chandrasekharam, M. Novel Carbazole-Phenothiazine Dyads for Dye-Sensitized Solar Cells: A Combined Experimental and Theoretical Study. *ACS Appl. Mater. Interfaces* **2013**, *5*, 9635−9647.
(39) Agrawal, S.; Leijtens, T.; Ronca, E.; Pastore, M.; Snaith, H.; De Angelis, F. Modeling the Effect of Ionic Additives on the Optical and Electronic Properties of a Dye-Sensitized $TiO_2$ Heterointerface: Absorption, Charge Injection and Aggregation. *J. Mater. Chem. A* **2013**, *1*, 14675−14685.
(40) Planells, M.; Pellejà, L.; Clifford, J. N.; Pastore, M.; De Angelis, F.; López, N.; Marder, S. R.; Palomares, E. Energy Levels, Charge Injection, Charge Recombination and Dye Regeneration Dynamics for Donor-Acceptor π-Conjugated Organic Dyes in Mesoscopic $TiO_2$ Sensitized Solar Cells. *Energy Environ. Sci.* **2011**, *4*, 1820−1829.
(41) Marotta, G.; Lobello, M. G.; Anselmi, C.; Barozzino Consiglio, G.; Calamante, M.; Mordini, A.; Pastore, M.; De Angelis, F. An Integrated Experimental and Theoretical Approach to the Spectroscopy of Organic-Dye-Sensitized $TiO_2$ Heterointerfaces: Disentangling the Effects of Aggregation, Solvation, and Surface Protonation. *ChemPhysChem* **2014**, *15*, 1116−1125.
(42) Zhang, L.; Cole, J. M. Adsorption Properties of P-Methyl Red Monomeric-to-Pentameric Dye Aggregates on Anatase (101) Titania Surfaces: First-Principles Calculations of Dye/$TiO_2$ Photoanode Interfaces for Dye-Sensitized Solar Cells. *ACS Appl. Mater. Interfaces* **2014**, *6*, 15760−15766.
(43) Kusama, H.; Sayama, K. Theoretical Study on the Intermolecular Interactions of Black Dye Dimers and Black Dye-Deoxycholic Acid Complexes in Dye-Sensitized Solar Cells. *J. Phys. Chem. C* **2012**, *116*, 23906−23914.
(44) Feng, S.; Li, Q.-S.; Yang, L.-N.; Sun, Z.-Z.; Niehaus, T. A.; Li, Z.-S. Insights into Aggregation Effects on Optical Property and Electronic Coupling of Organic Dyes in Dye Sensitized Solar Cells. *J. Power Sources* **2015**, *273*, 282−289.
(45) Seifert, G. Tight-Binding Density Functional Theory: An Approximate Kohn-Sham DFT Scheme†. *J. Phys. Chem. A* **2007**, *111*, 5609−5613.
(46) Elstner, M.; Porezag, D.; Jungnickel, G.; Elsner, J.; Haugk, M.; Frauenheim, T.; Suhai, S.; Seifert, G. Self-Consistent-Charge Density-Functional Tight-Binding Method for Simulations of Complex Materials Properties. *Phys. Rev. B: Condens. Matter Mater. Phys.* **1998**, *58*, 7260−7268.
(47) Becke, A. D. Density-Functional Thermochemistry. III. The Role of Exact Exchange. *J. Chem. Phys.* **1993**, *98*, 5648−5652.
(48) Grimme, S. Accurate Description of Van Der Waals Complexes by Density Functional Theory Including Empirical Corrections. *J. Comput. Chem.* **2004**, *25*, 1463−1473.
(49) Becke, A. D. A New Mixing of Hartree-Fock and Local Density-Functional Theories. *J. Chem. Phys.* **1993**, *98*, 1372−1377.
(50) Goerigk, L.; Grimme, S. A Thorough Benchmark of Density Functional Methods for General Main Group Thermochemistry, Kinetics, and Noncovalent Interactions. *Phys. Chem. Chem. Phys.* **2011**, *13*, 6670−6688.
(51) Aradi, B.; Hourahine, B.; Frauenheim, T. DFTB+, a Sparse Matrix-Based Implementation of the DFTB Method†. *J. Phys. Chem. A* **2007**, *111*, 5678−5684.
(52) Niehaus, T. A.; Elstner, M.; Frauenheim, T.; Suhai, S. Application of an Approximate Density-Functional Method to Sulfur Containing Compounds. *J. Mol. Struct.: THEOCHEM* **2001**, *541*, 185−194.
(53) Gaus, M.; Cui, Q.; Elstner, M. DFTB3: Extension of the Self-Consistent-Charge Density-Functional Tight-Binding Method (SCC-DFTB). *J. Chem. Theory Comput.* **2011**, *7*, 931−948.


DOI: 10.1021/acsami.5b06743
*ACS Appl. Mater. Interfaces* 2015, 7, 22504−22514

(54) Dolgonos, G.; Aradi, B. l.; Moreira, N. H.; Frauenheim, T. An Improved Self-Consistent-Charge Density-Functional Tight-Binding (SCC-DFTB) Set of Parameters for Simulation of Bulk and Molecular Systems Involving Titanium. *J. Chem. Theory Comput.* **2010**, *6*, 266−278.
(55) Tsai, H.-H. G.; Tan, C.-J.; Tseng, W.-H. Electron Transfer of Squaraine-Derived Dyes Adsorbed on $TiO_2$ Clusters in Dye-Sensitized Solar Cells: A Density Functional Theory Investigation. *J. Phys. Chem. C* **2015**, *119*, 4431−4443.
(56) Cossi, M.; Rega, N.; Scalmani, G.; Barone, V. Energies, Structures, and Electronic Properties of Molecules in Solution with the C-PCM Solvation Model. *J. Comput. Chem.* **2003**, *24*, 669−681.
(57) Frisch, M. J.; Trucks, G. W.; Schlegel, H. B.; Scuseria, G. E.; Robb, M. A.; Cheeseman, J. R.; Scalmani, G.; Barone, V.; Mennucci, B.; Petersson, G. A.; Nakatsuji, H.; Caricato, M.; Li, X.; Hratchian, H. P.; Izmaylov, A. F.; Bloino, J.; Zheng, G.; Sonnenberg, J. L.; Hada, M.; Ehara, M.; Toyota, K.; Fukuda, R.; Hasegawa, J.; Ishida, M.; Nakajima, T.; Honda, Y.; Kitao, O.; Nakai, H.; Vreven, T.; Montgomery, J. A., Jr.; Peralta, J. E.; Ogliaro, F.; Bearpark, M.; Heyd, J. J.; Brothers, E.; Kudin, K. N.; Staroverov, V. N.; Kobayashi, R.; Normand, J.; Raghavachari, K.; Rendell, A.; Burant, J. C.; Iyengar, S. S.; Tomasi, J.; Cossi, M.; Rega, N.; Millam, J. M.; Klene, M.; Knox, J. E.; Cross, J. B.; Bakken, V.; Adamo, C.; Jaramillo, J.; Gomperts, R.; Stratmann, R. E.; Yazyev, O.; Austin, A. J.; Cammi, R.; Pomelli, C.; Ochterski, J. W.; Martin, R. L.; Morokuma, K.; Zakrzewski, V. G.; Voth, G. A.; Salvador, P.; Dannenberg, J. J.; Dapprich, S.; Daniels, A. D.; Farkas, O.; Foresman, J. B.; Ortiz, J. V.; Cioslowski, J.; Fox, D. J. *Gaussian 09*, revision D.01; Gaussian, Inc.: Wallingford CT, 2009.
(58) Kirkpatrick, J. An Approximate Method for Calculating Transfer Integrals Based on the Zindo Hamiltonian. *Int. J. Quantum Chem.* **2008**, *108*, 51−56.
(59) Yang, X.-D.; Li, Q.-K.; Shuai, Z.-G. Theoretical Modelling of Carrier Transports in Molecular Semiconductors: Molecular Design of Triphenylamine Dimer Systems. *Nanotechnology* **2007**, *18*, 424029.
(60) Yin, S.-W.; Yi, Y.-P.; Li, Q.-X.; Yu, G.; Liu, Y.-Q.; Shuai, Z.-G. Balanced Carrier Transports of Electrons and Holes in Silole-Based Compoundsa Theoretical Study. *J. Phys. Chem. A* **2006**, *110*, 7138−7143.
(61) Troisi, A.; Orlandi, G. The Hole Transfer in DNA: Calculation of Electron Coupling between Close Bases. *Chem. Phys. Lett.* **2001**, *344*, 509−518.
(62) Nan, G.-J.; Wang, L.-J.; Yang, X.-D.; Shuai, Z.-G.; Zhao, Y. Charge Transfer Rates in Organic Semiconductors Beyond First-Order Perturbation: From Weak to Strong Coupling Regimes. *J. Chem. Phys.* **2009**, *130*, 024704.
(63) Rodriguez-Monge, L.; Larsson, S. Conductivity in Polyacetylene. 3. Ab Initio Calculations for a Two-Site Model for Electron Transfer. *J. Phys. Chem.* **1996**, *100*, 6298−6303.
(64) Kosar, B.; Albayrak, C. Spectroscopic Investigations and Quantum Chemical Computational Study of (E)-4-Methoxy-2-[(P-Tolylimino)Methyl]Phenol. *Spectrochim. Acta, Part A* **2011**, *78*, 160−167.
(65) Anselmi, C.; Mosconi, E.; Pastore, M.; Ronca, E.; De Angelis, F. Adsorption of Organic Dyes on $TiO_2$ Surfaces in Dye-Sensitized Solar Cells: Interplay of Theory and Experiment. *Phys. Chem. Chem. Phys.* **2012**, *14*, 15963−15974.
(66) Sun, P.-P.; Li, Q.-S.; Yang, L.-N.; Sun, Z.-Z.; Li, Z.-S. Theoretical Investigation on Structural and Electronic Properties of Organic Dye C258 on $TiO_2$(101) Surface in Dye-Sensitized Solar Cells. *Phys. Chem. Chem. Phys.* **2014**, *16*, 21827−21837.
(67) Clifford, J. N.; Palomares, E.; Nazeeruddin, M. K.; Grätzel, M.; Nelson, J.; Li, X.; Long, N. J.; Durrant, J. R. Molecular Control of Recombination Dynamics in Dye-Sensitized Nanocrystalline $TiO_2$ Films: Free Energy vs Distance Dependence. *J. Am. Chem. Soc.* **2004**, *126*, 5225−5233.
(68) Haque, S. A.; Handa, S.; Peter, K.; Palomares, E.; Thelakkat, M.; Durrant, J. R. Supermolecular Control of Charge Transfer in Dye-Sensitized Nanocrystalline $TiO_2$ Films: Towards a Quantitative Structure-Function Relationship. *Angew. Chem., Int. Ed.* **2005**, *44*, 5740−5744.
(69) Johnson, E. R.; Keinan, S.; Mori-Sánchez, P.; Contreras-García, J.; Cohen, A. J.; Yang, W. Revealing Noncovalent Interactions. *J. Am. Chem. Soc.* **2010**, *132*, 6498−6506.
(70) Qi, D.-D.; Zhang, L.-J.; Wan, L.; Zhao, L.-Y.; Jiang, J.-Z. Design of a Universal Reversible Bidirectional Current Switch Based on the Fullerene-Phthalocyanine Supramolecular System. *J. Phys. Chem. A* **2012**, *116*, 6785−6791.


DOI: 10.1021/acsami.5b06743
*ACS Appl. Mater. Interfaces* 2015, 7, 22504−22514